Impact of radiation and electron trapping on minority carrier transport in p -Ga2O3

Sushrut Modak, Alfons F. Schulte, Corinne Sartel, Vincent Sallet, Yves Dumont, Ekaterine Chikoidze, Xinyi Xia, Fan Ren, S. J. Pearton, Ariel Ruzin, et al.

Impact of radiation and electron injection on minority carrier transport in *p*-Ga_2O_3

Sushrut Modak [a)], Alfons Schulte [a)], Corinne Sartel [b)], Vincent Sallet [b)], Yves Dumont [b)], Ekaterine Chikoidze [b)], Xinyi Xia [c)], Fan Ren [c)], Stephen J. Pearton [d)], Arie Ruzin [e)] and Leonid Chernyak [a,f)]

[a] *Department of Physics, University of Central Florida, Orlando, FL 32816, USA*

[b] *Groupe d'Etude de la Matière Condensée, Université Paris-Saclay, Université de Versailles Saint Quentin en Yvelines – CNRS, 45 Av. des Etats-Unis, 78035 Versailles Cedex, France*

[c] *Department of Chemical Engineering, University of Florida, Gainesville, FL 32611, USA*

[d] *Material Science and Engineering, University of Florida, Gainesville, FL 32611, USA*

[e] *School of Electrical Engineering, Tel Aviv University, Tel Aviv 69978, Israel*

Highly resistive undoped p-type Gallium Oxide samples were subjected to cumulative proton irradiation with energies ranging from 25 keV to 70 keV and doses in the $1.6x10^{14}$ cm^{-2} – $3.6x10^{14}$ cm^{-2} range. Proton irradiation resulted in up to a factor of 2 reduction of minority electron diffusion length in the samples for temperatures between ~ 300 and 400 K. Electron injection into the samples under test using the beam of a Scanning Electron Microscope leads to pronounced elongation of diffusion length beyond the pre-irradiation values, thus demonstrating stable (days after injection) recovery of adverse radiation impact on minority carrier transport. The activation energy of 91 meV, estimated from the temperature dependent diffusion length versus electron injection duration experiments, is likely related to the local potential barrier height for native defects associated with the phenomenon of interest.

[f)] email: chernyak@physics.ucf.edu

The main limiting factor in Ga_2O_3 technology is related to difficulties of p-type conductivity realization [1-4]. Previous studies indicate that holes in β-Ga_2O_3 have characteristics of low dispersion, high effective mass and high density of states. This results in formation of weak polarons (or localized holes), trapped by lattice distortions [5-9], hindering p-type conductivity. Contradicting to these claims, ref. [3] has experimentally shown a possibility of low p-type intrinsic conductivity in Ga_2O_3. It is additionally reported that the self-trapping nature of holes practically disappears at temperatures above 90-120 K [4]. Given the current state-of-the-art and ever mounting interest in p-Ga_2O_3, one can reasonably claim that a robust p-type Ga_2O_3 electrical conductivity, will be possible in the foreseeable future, in addition to the use of heterojunction p-n junctions [10].

In Ga_2O_3, once bipolar devices become available, minority carrier transport (diffusion length) will be of primary importance. Minority carrier diffusion length defines performance of bipolar devices such as p-n junction diodes, bipolar transistors, and p-*i*-n detectors [11]. One of the major issues in the current ZnO and GaN device technology, is the low diffusion length of minority carriers, partially due to dislocation scattering [12, 13]. It has been previously shown that in p-type GaN and ZnO, low energy electron injection, either with an electron beam of Scanning Electron Microscope (SEM) or forward bias, results in a significant increase of the minority carrier (electron) diffusion length [12, 14-17]. Similar effects have been very recently observed in n-type Ga_2O_3 subjected to low energy electron beam injection [18-20].

This paper studies minority carrier transport (electron diffusion length) in p-Ga_2O_3 highly resistive samples subjected to proton irradiation following injection from an SEM electron beam. The below-presented results demonstrate feasibility for a significant diffusion length increase

beyond the initial pre-irradiated values, thus paving the road towards solid-state electron injection in the future Ga_2O_3 bipolar devices.

Undoped β-Ga_2O_3 samples, analyzed in this study, were grown in a RF-heated horizontal MOCVD reactor. Trimethylgallium (TMGa) and 5.5 N pure oxygen were used as gallium and oxygen sources, respectively. Argon was used as the carrier gas (cf. ref. [21]). The β-Ga_2O_3 layer was grown on c-oriented sapphire substrate using Ga/O ratio and growth temperature as 1.4×10^{-4} and 775 °C, respectively. The total reactor pressures of 30-38 Torr and variable growth rates (gallium and oxygen precursor fluxes) were used to have different native defect (V_{Ga} and V_o) concentrations in the Ga_2O_3 films, leading to the different values of hole concentrations.. The epitaxial layer thickness was ~ 450 nm. X-ray diffraction revealed highly textured films of gallium oxide in the β-Ga_2O_3 phase with monoclinic space group (*C2/m*) symmetry.

Ohmic contacts for electrical characterization were prepared by silver paint at the four corners of the sample. Hall Effect measurements were performed in a Van der Pauw configuration in the 500-850 K temperature range for magnetic fields perpendicular to the film plane varying from -1.6 to 1.6 T, using a high impedance high temperature custom-designed measurement set-up. Resistivities at highest measured T = 850 K were found in the range from 1.2×10^3 Ohm·cm to 1.3×10^4 Ohm·cm. Hall Effect measurements demonstrated the positive sign for majority carriers in both samples, thus confirming the p-type conductivity. The free hole concentrations and mobilities at 850 K were estimated in 10^{13} - 5.6×10^{14} cm^{-3} range and 8 - 16 $cm^2V^{-1}s^{-1}$ range, respectively. More details could be found elsewhere [22].

Minority carrier diffusion length (L) measurements were carried out using Electron Beam-Induced Current (EBIC) technique *in-situ* in Phillips XL-30 Scanning Electron Microscope (SEM). Details on EBIC techniques could be found in refs. [12, 13, 22]. The measurements were

carried out in the temperature range of 294-404 K using temperature-controlled stage integrated into the SEM. For EBIC measurements, electron beam energy was kept at 10 keV. The EBIC line-scans for diffusion length extraction were carried out in planar configuration using Ni/Au (20 nm/ 80 nm) asymmetrical pseudo-Schottky contacts created on the film with lithography/liftoff techniques. Single line-scan takes approximately 12 seconds, which is sufficient for extraction of minority carrier diffusion length value. To perform electron injection in the region of EBIC measurements, line-scans were not interrupted for the total time of up to 400 seconds. The values of diffusion length were extracted intermittently. EBIC signal was amplified with Stanford Research Systems SR 570 low-noise current amplifier and digitized with Keithley DMM 2000 controlled by a PC using a home-made software.

Cathodoluminescence (CL) measurements were carried out under 10 kV accelerating voltage using Gatan MonoCL2 attachment to the SEM. Spectra were recorded with a Hamamatsu photomultiplier tube sensitive in 150-850 nm range and single grating monochromator (blazed at 1200 lines/mm).

Ga_2O_3 samples were irradiated with protons having a dose/energy sequence to create a near-uniform hydrogen concentration around 10^{19} cm^{-3}. This consisted of 25 keV/1.6 $x10^{14}$ cm^{-2}, 50 keV/1.7$x10^{14}$ cm^{-2} and 70 keV/3.6$x10^{14}$ cm^{-2}. EBIC and CL measurements were carried out before and after proton irradiation and the results were compared.

The temperature dependence of L before and after proton irradiation is shown in Fig. 1. L decreased with increasing temperature with room temperature values being at 1200 and 630 nm, respectively. Relatively large values of L are partially due to the very low majority carrier concentration. Within the current temperature range of measurements, it is likely that the origin of L decrease is due to phonon scattering [22].

The activation energy for temperature dependence of L is given by [12, 22]:

$$L(T) = L_0 \exp\left(\frac{\Delta E_{A,T}}{2kT}\right). \quad (1)$$

Here, L_0 is a scaling constant, $\Delta E_{A,T}$ is the thermal activation energy, k is the Boltzmann constant, and T is the temperature. The activation energy pertaining to the reduction of L with temperature is estimated at 76 meV after irradiation (113 meV pre-irradiation). A detailed discussion regarding the origin of $\Delta E_{L,T}$ is presented in ref. [22].

Fig. 2 presents results of the electron injection experiments carried out at variable temperature. Minority electron diffusion length exhibits a linear increase with duration of electron injection before saturation occurs (not shown in Fig. 2). The linear increase of L with electron injection duration was previously observed in p-GaN [14], p-ZnO [11], unintentionally doped GaN [23] and n-Ga_2O_3 [18]. Minority carrier diffusion length increase in Fig. 2 is characterized by the rate R (dL/dt; where t is duration of electron injection), which drops from 1.6 nm/s at room temperature to about 0.9 nm/s at 120 ^oC.

The effect of temperature on rate R is described by [22]:

$$R(T) = R_0 \exp\left(\frac{\Delta E_{A,T}}{2kT}\right) \exp\left(\frac{\Delta E_{A,I}}{kT}\right). \quad (2)$$

Here R_0 is a scaling constant and $\Delta E_{A,I}$ is the electron injection effect activation energy. Equation (2) can be used to find the activation energy of injection-induced component for the increase in L from the Arrhenius plot in the inset of Fig. 3. The latter figure shows R decrease with increasing temperature. The slope of the Arrhenius plot is $\Delta E_{A,I}$ + 0.5 $\Delta E_{A,T}$, from which $\Delta E_{A,I}$ ~ 91 meV is obtained. $\Delta E_{A,I}$ is associated with the mechanism responsible for the elongation of L with injected charge. The latter effect is likely associated with gallium vacancy (V_{Ga}), which is a pervasive point defect in undoped Ga_2O_3.

Detailed mechanism for the electron injection-induced L increase is presented in ref. [22] for undoped GaN. This mechanism is also applicable to p-Ga_2O_3 and its key points are outlined as follows:

- A non-equilibrium electron, generated by a Scanning Electron Microscope beam gets trapped by gallium vacancies, which are deep acceptors in Ga_2O_3 [23]. Because of its energetic position in Ga_2O_3 forbidden gap and fairly large concentration in the material (~ 10^{18} cm^{-3}) a pronounced number of V_{Ga} remains in neutral state, thus acting as meta-stable electron trap. Trapping non-equilibrium electrons on the V_{Ga}-levels prevents recombination of the conduction band electrons through these levels. This leads to an increase of lifetime, τ, for a non-equilibrium electron in the conduction band and, as a result, to an increase of L ($L = (D\tau)^{1/2}$, where D is carrier diffusivity).
- The V_{Ga}-level containing a trapped electron becomes again available for recombination of a non-equilibrium conduction band electron as this level captures a hole. Capturing a hole means a transition of the trapped electron to the valence band. The rate of this transition increases with increasing temperature, and one notes the existence of the activation energy, preventing the immediate hole capture by negatively charged gallium vacancy. This activation energy is $\Delta E_{A,I,}$ experimentally estimated at 91 meV.
- As the rate of hole capture on the V_{Ga}-level increases, the conduction band electrons have more chance for recombination on this level. This results in a shorter non-equilibrium minority electron lifetime and a slower rate for L increase at higher temperatures as seen in Fig. 2.

The results in Fig. 2 demonstrate that the adverse impact of proton irradiation can be fully recovered due to electron injection and the diffusion length in the irradiated material can increase even beyond the pre-irradiation values at respective temperatures. Stability of electron injection-

induced increase of diffusion length was studied at room temperature after stopping the electron injection (up to 400 seconds total time at each temperature). It has been found that the increased diffusion length stays unchanged for at least several days.

Fig. 4 demonstrates normalized room temperature CL spectra before and after proton irradiation. Detailed studies of p-Ga_2O_3 optical properties prior to irradiation were recently presented in ref. [22]. Narrowing of CL spectrum after proton irradiation in Fig. 4 is likely related to a variety of complexes, created between V_{Ga} and implanted hydrogen. These complexes may reduce strain-induced broadening of the CL peaks [23]. CL measurements after electron injection into proton-irradiated Ga_2O_3 did not reveal any additional changes in the spectrum (both in terms of shape and intensity), indicating that the injection-induced increase of non-equilibrium carrier lifetime is mostly non-radiative in nature.

In summary, electron injection from SEM beam was employed to "heal" the adverse impact of proton irradiation on minority carrier transport in p-type Ga_2O_3. The obtained results demonstrate that reduction of the diffusion length due to irradiation could be fully recovered, and L can even exceed the pre-irradiation values. The effect was ascribed to non-equilibrium electron trapping on native defects (V_{Ga}) and consequent increase of minority carrier (electron) lifetime in the conduction band of Gallium Oxide. Once Ga_2O_3 p-n junctions become available, a solid-state electron injection due to forward-bias (injection of electrons from n-side of p-n junction into p-side due to applying a negative voltage to n-type material) will be attempted, thus paving the road towards purely electrical (athermal) mitigation of radiation-induced defects in bipolar devices. This type of defect mitigation does not require high temperature annealing or changes in technological processes, which are both costly. Additionally, based on the results obtained so far,

the process of electron injection requires only seconds, while the induced improvements of minority carrier transport are stable for days.

Acknowledgements

The research at UCF was supported in part by NSF (ECCS1802208 and ECCS2127916). Research at UCF and Tel Aviv University was supported in part by the US-Israel BSF (award # 2018010) and NATO (award # G5748). The work at UF was performed as part of the Interaction of Ionizing Radiation with Matter University Research Alliance (IIRM-URA**)**, sponsored by the Department of the Defense, Defense Threat Reduction Agency under award HDTRA1-20-2-0002, monitored by Jacob Calkins and by NSF DMR 1856662 (J.H. Edgar). The present work is a part of "GALLIA" International Research Project, CNRS, France.

Data Availability

The data that supports the findings of this study is available within the article.

References

1. A. Mock, R. Korlacki, C. Briley, V. Darakchieva, B. Monemar, Y. Kumagai, K. Goto, M. Higashiwaki, and M. Schubert, Physical Review B **96**, 14 (2017).
2. S.I. Stepanov, V. I. Nikolaev, V. E. Bougrov, and A. E. Romanov, Review of Advanced Material Science **44**, 63 (2016).
3. E. Chikoidze, C. Sartel, H. Mohamed, I. Madaci, T. Tchelidze, M. Modreanu, P. Vales-Castro, C. Rubio, C. Arnold, V. Sallet, Y. Dumont, and A. Perez-Tomas, J. Mater. Chem. C **7**, 10231 (2019)
4. B.E. Kananen, N.C. Giles, L.E. Halliburton, G.K. Foundos, K.B. Chang, and K.T. Stevens, J. Appl. Phys. **122**, 6 (2017).
5. J.B. Varley, A. Janotti, C. Franchini, and C.G. Van de Walle, Physical Review B **85**, 081109 (2012).
6. A. Goyal, A. Zakutayev, V. Stevanović, and S. Lany, J. Appl. Phys. **129**, 245704 (2021).
7. H. He, R. Orlando, M.A. Blanco, R. Pandey, E. Amzallag, I. Baraille, and M. Rérat, Physical Review B **74**, 8 (2006).
8. H. He, M.A. Blanco, and R. Pandey, Appl. Phys. Lett. **88**, 261904 (2006).
9. J. Furthmüller and F. Bechstedt, Physical Review B **93**, 16 (2016).
10. Jiaye Zhang, Shaobo Han, Meiyan Cui, Xiangyu Xu, Weiwei Li, Haiwan Xu, Cai Jin, Meng Gu, Lang Chen and Kelvin H. L. Zhang, ACS Appl. Electron. Mater. 2, 456 (2020).
11. L. Chernyak and A. Schulte, Method and System for Performance Improvement of Photodetectors and Solar Cells, U.S. Patent #6,674,064, January 6, 2004.
12. O. Lopatiuk-Tirpak, L. Chernyak, F.X. Xiu, J.L. Liu, S. Jang, F. Ren, S.J. Pearton, K. Gartsman, Y. Feldman, A. Osinsky, and P. Chow, J. Appl. Phys. **100**, 086101 (2006).
13. L. Chernyak, A. Osinsky, G. Nootz, A. Schulte, J. Jasinski, M. Benamara, and Z. Liliental-Weber, D. C. Look, R. J. Molnar, Appl. Phys. Lett. **77**, 2695 (2000).
14. L. Chernyak, G. Nootz, and A. Osinsky, Electronics Letters **37**, 922 (2001).

15. L. Chernyak, A. Osinsky, V. Fuflyigin, and E.F. Schubert, Appl. Phys. Lett. **77**, 875 (2000).

16. O. Lopatiuk-Tirpak, L. Chernyak, Y. L. Wang, F. Ren, S. J. Pearton, K. Gartsman, and Y. Feldman, Appl. Phys. Lett. **90**, 3 (2007).

17. O. Lopatiuk-Tirpak, L. Chernyak, L.J. Mandalapu, Z. Yang, J.L. Liu, K. Gartsman, Y. Feldman, and Z. Dashevsky, Appl. Phys. Lett. **89**, 142114 (2006).

18. S. Modak, L. Chernyak, S. Khodorov, I. Lubomirsky, A. Ruzin, M. Xian, F. Ren, and S.J. Pearton, ECS J. Solid State Sci. Technol. **9**, 045018 (2020).

19. S. Modak, J. Lee, L. Chernyak, J. Yang, F. Ren, S.J. Pearton, S. Khodorov, and I. Lubomirsky, AIP Advances **9**, 015127 (2019).

20. S. Modak, L. Chernyak, S. Khodorov, I. Lubomirsky, J. Yang, F. Ren, and S.J. Pearton, ECS J. Solid State Sci. Technol. **8**, Q3050-Q3053 (2019).

21. E. Chikoidze, C. Sartel, H. Mohamed, I. Madaci, T. Tchelidze, M. Modreanu, P. Vales-Castro, C. Rubio, C. Arnold, V. Sallet, Y. Dumont, and A. Perez-Tomas, Journal of Materials Chemistry C **7**, 10231-10239 (2019).

22. S. Modak, L. Chernyak, A. Schulte, C. Sartel, V. Sallet, Y. Dumont, E. Chikoidze, X. Xia, F. Ren, S.J. Pearton, A. Ruzin, D.M. Zhigunov, S.S. Kosolobov, and V.P. Drachev, APL Mater **10**, 031106 (2022).

23. S. Modak, L. Chernyak, M.H. Xian, F. Ren, S.J. Pearton, S. Khodorov, I. Lubomirsky, A. Ruzin, and Z. Dashevsky, J. Appl. Phys. **128**, 085702 (2020).

24. A. Karjalainen, P.M. Weiser, I. Makkonen, V.M. Reinertsen, L. Vines, and F. Tuomisto, J. Appl. Phys. **129**, 165702 (2021).

Figure Captions

Figure 1:

Temperature dependence of diffusion length in the structure before and after irradiation with high energy protons (25 keV 1.6 x10^{14} cm^{-2} + 50 keV, 1.7x10^{14} cm^{-2} + 70 keV, 3.6x10^{14} cm^{-2}).

Figure 2:

The change in diffusion length as a function of duration of electron injection for temperatures in 294-393 K range. Pre-irradiation diffusion length values are shown in red color. The activation energy $\Delta E_{A,I}$, obtained from L dependence on electron injection duration at variable temperature, is estimated at 91 meV using equation (2).

Figure 3:

Temperature dependence of the rate (R) for change in L with time. **Inset**: Arrhenius plot of equation (2) for calculation of activation energy for the effect of electron injection.

Figure 4:

Normalized room-temperature cathodoluminescence spectrum before and after proton irradiation. A slight blue shift of the irradiation peak with smaller full width at half-maxima was observed after irradiation.

Figure 1

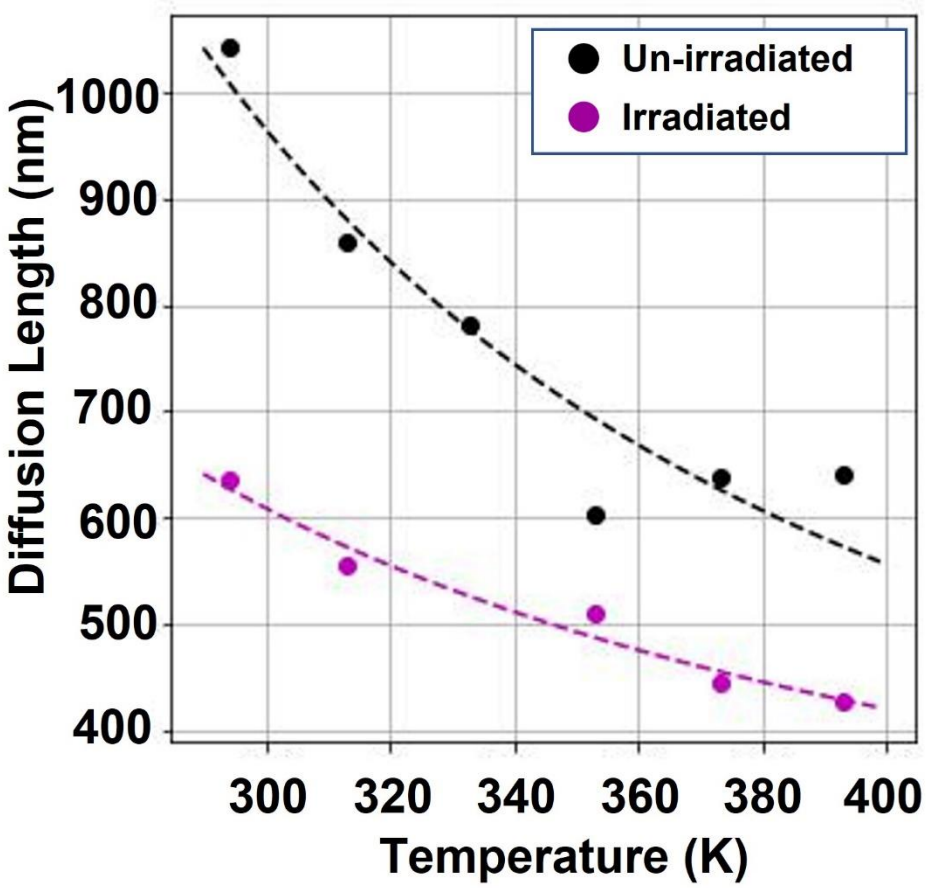
Un-irradiated
Irradiated
Diffusion Length (nm)
1000
900
800
700
600
500
400
300
320
340
360
380
400
Temperature (K)

Figure 2

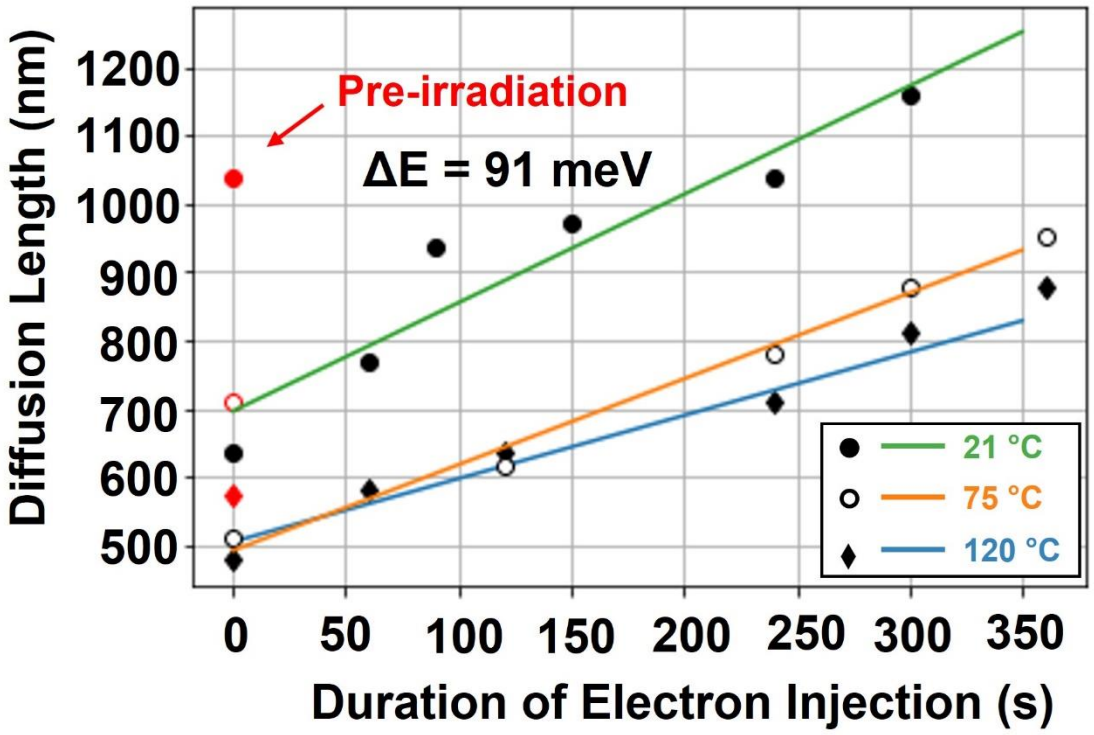
Diffusion Length (nm)
1200
1100
1000
900
800
700
600
500
Pre-irradiation
ΔE = 91 meV
21 °C
75 °C
120 °C
0
50
100
150
200
250
300
350
Duration of Electron Injection (s)

Figure 3

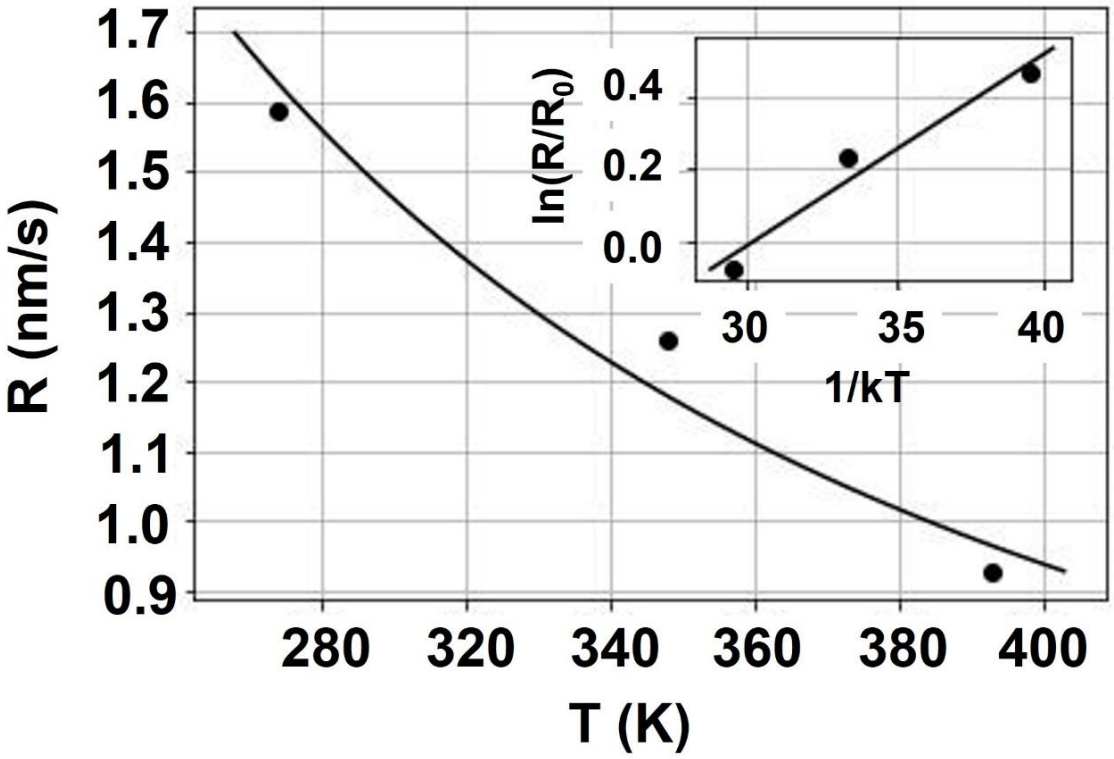
R (nm/s)
1.7
1.6
1.5
1.4
1.3
1.2
1.1
1.0
0.9
280
320
340
360
380
400
T (K)
ln(R/R0)
0.4
0.2
0.0
30
35
40
1/kT

Figure 4

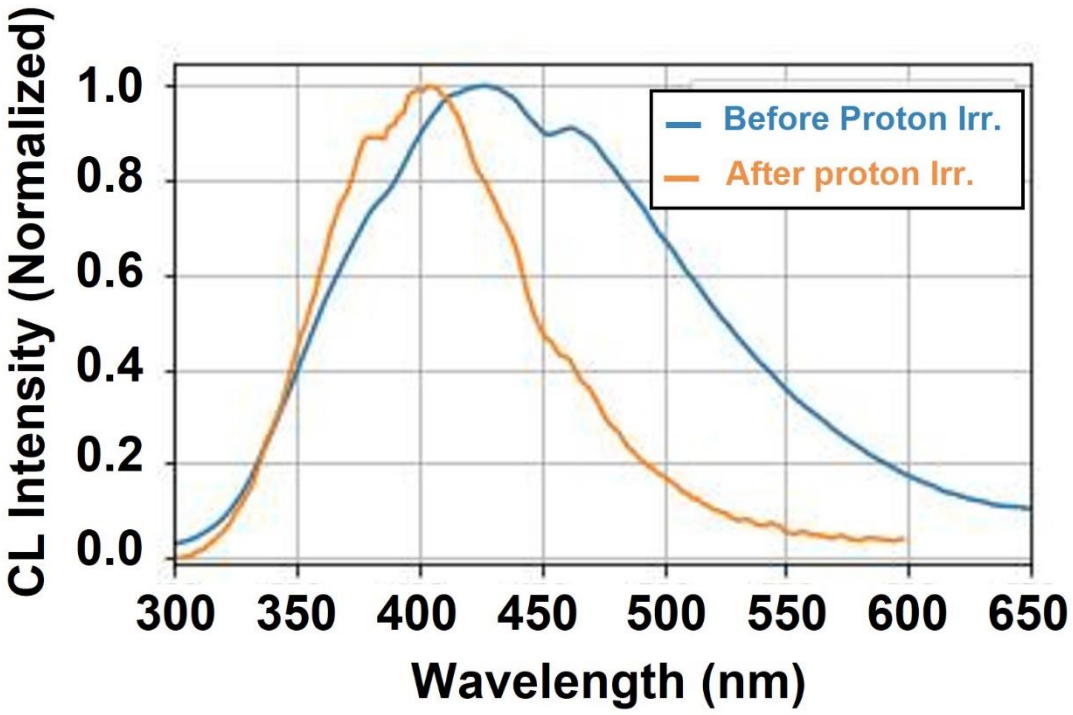
CL Intensity (Normalized)
1.0
0.8
0.6
0.4
0.2
0.0
300
350
400
450
500
550
600
650
Wavelength (nm)
Before Proton Irr.
After proton Irr.